Composites Part B 77 (2015) 199–208

Contents lists available at ScienceDirect

Composites Part B

journal homepage: www.elsevier.com/locate/compositesb

Interfacial shear strength estimates of NiTi–Al matrix composites fabricated via ultrasonic additive manufacturing

Adam Hehr, Marcelo J. Dapino*

Smart Vehicle Concepts Center, Department of Mechanical and Aerospace Engineering, The Ohio State University, 201 W 19th Ave, Columbus, OH, 43210, USA

ARTICLE INFO

Article history:
Received 27 June 2014
Received in revised form
2 February 2015
Accepted 3 March 2015
Available online 12 March 2015

Keywords:
A. metal-matrix composites (MMCs)
Shape memory alloys
B. Fibre/matrix bond
C. Finite element analysis (FEA)
D. Mechanical testing

ABSTRACT

The purpose of this study is to understand and improve the interfacial shear strength of metal matrix composites fabricated via ultrasonic additive manufacturing (UAM). NiTi–Al composites can exhibit dramatically lower thermal expansion compared to aluminum, yet blocking stresses developed during thermal cycling have been found to degrade and eventually cause interface failure in these composites. In this study, the strength of the interface was characterized with pullout tests. Since adhered aluminum was consistently observed on all pullout samples, the matrix yielded prior to the interface breaking. Measured pullout loads were utilized as an input to a finite element model for stress and shear lag analysis. The aluminum matrix experiences a calculated peak shear stress near 230 MPa, which is above its ultimate shear strength of 150–200 MPa thus corroborating the experimentally-observed matrix failure. The influence of various fiber surface treatments and consolidation characteristics on bond mechanisms was studied with scanning electron microscopy, energy dispersive X-ray spectroscopy, optical microscopy, and focused ion beam microscopy.

1. Problem statement and introduction

Ultrasonic additive manufacturing (UAM) is a recently developed rapid prototyping process where thin foils of similar or dissimilar metals are ultrasonically welded together in a layer by layer process to form gap-less, 3D metal parts [1]. Along with welding, periodic machining is utilized during the UAM process to implement complex designs, features, and to remove material for embedding various objects into the structure, such as reinforcing fibers. A schematic of the UAM process is shown in Fig. 1.

Due to the physics of ultrasonic welding, metallic bonding takes place at temperatures far below metallic melting temperatures. Thus, temperature sensitive materials such as nickel titanium (NiTi) shape memory alloys can be combined or built into metallic structures. Current UAM systems utilize 9 kW of ultrasonic power, nearly an order of magnitude higher than early UAM equipment. The increase in weld power allows for higher process down force and higher quality interfacial properties between foils and between foils and embedded fibers [2].

Recently, UAM has been utilized to fabricate aluminum matrix composites with embedded NiTi shape memory alloy fibers for thermally invariant components. Specifically, when the composite is heated, the strain recovery of the NiTi fibers counteracts the expansion of the aluminum matrix. This combination creates a low density, stiff, and thermally stable material for engineering applications. Previous efforts have shown a 60% reduction in the average coefficient of thermal expansion for Al 3003 up to 100 °C [3]. Yet, metallic bonding between the aluminum matrix and NiTi fibers is not always observed. Instead, the interface is believed to be predominately supported by mechanical coupling in the form of a friction fit [4]. Although it is desirable to achieve metallic bonding at the interface, mechanical coupling may be sufficient if the interface strength exceeds thermal blocking stresses generated throughout temperature cycling. However, previous efforts have shown evidence of interface failure when significant blocking stresses arise [4].

To further investigate the high temperature interface failure, interfacial shear stresses of NiTi–Al 6061 composites are estimated through single fiber pullout tests [5]. Understanding the strength and failure characteristics of the interface is critical for designing reliable and robust NiTi composites. Pullout testing has been found to be effective in estimating interface strength and understanding failure behavior in polymeric composites with embedded NiTi

* Corresponding author. Tel.: +1 614 688 3689.
E-mail address: dapino.1@osu.edu (M.J. Dapino).

http://dx.doi.org/10.1016/j.compositesb.2015.03.005
1359-8368/

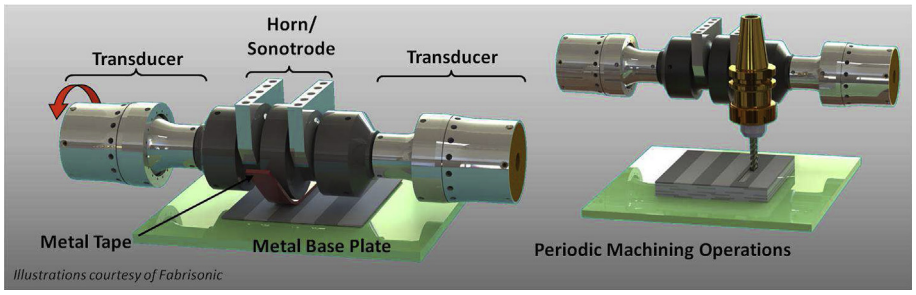

Fig. 1. Ultrasonic additive manufacturing process for developing novel and unique metal composites and designs.

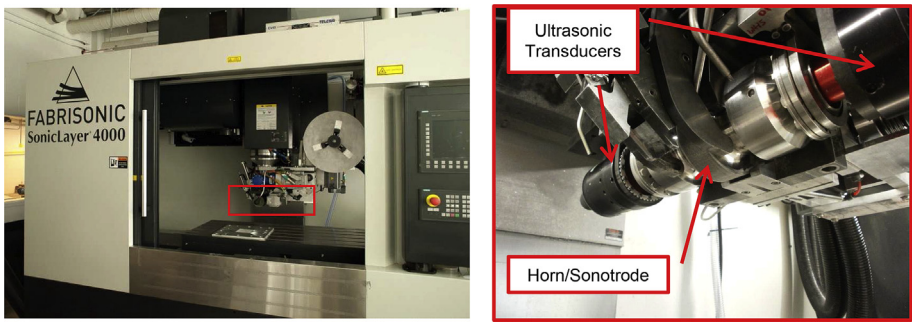

Fig. 2. Current 9 kW UAM system with sonotrode and ultrasonic welder assembly boxed in red. (For interpretation of the references to color in this figure legend, the reader is referred to the web version of this article.)

[6–13]. In addition to estimating strength, the influence of various surface treatments on the NiTi fibers was investigated for possible improvement of the interface strength and bonding behavior. The surface treatments investigated are as-built oxide (past surface finish of use and control), chemically etched, mechanically polished, and mechanically roughened. The chemically etched and mechanically polished finish increase the likelihood that metallic bonding may take place due to the as-built oxide layer being removed. On the other hand, the mechanically roughened surface would potentially increase the mechanical interlocking and increase the likelihood of metallic bonding. To complement the fiber pullout tests, scanning electron microscopy (SEM) and energy dispersive X-ray spectroscopy (EDS) were utilized to compare and contrast bond type and quality for each NiTi surface finish. Additionally, optical microscopy and focused ion beam (FIB) microscopy were utilized to analyze interface failure behavior and matrix microstructure around embedded fibers.

2. Methods

2.1. Sample manufacture

In this study, Al 6061-H18[1] was utilized as the metal matrix for the NiTi–Al UAM composites. Al 6061 was chosen due to its frequent use in industry and strong compatibility with UAM. Samples were manufactured on a 9 kW UAM system [14], Fig. 2. The machine has a fully automated tape feed, a computer numerical control (CNC) stage, and a laser machining stage to complement the ultrasonic welder.

The NiTi fiber diameter utilized in this study, for all surface finish types, was 0.28 mm (0.011″), as supplied by Nitinol Devices and Components, Inc. The material was shape-set to be straight and was super-elastic prior to embedding (Austenite finish temperature above room temperature). Super-elastic fibers were selected due to available material supply. Welding was performed with a 7 micron Ra surface roughness sonotrode on 101.6 mm by 76.2 mm (4″ by 3″) Al 6061-T6 base plates near 4.76 mm (0.1875″) in thickness. The base plates were constrained with a custom metal matrix composite fabrication fixture and vacuum chuck. Foils with a width of 23.81 mm (15/16″) and a thickness of 0.152 mm (0.006″) were utilized. The welding parameters used in this study are listed in Table 1. These parameters were chosen from a statistical optimization study for UAM-welded Al 6061-H18 material [15].

Table 1
Ultrasonic welding parameters used in this study.

Parameter	Value
Temperature	22 °C (70 °F)
Force	6000 N
Amplitude	32.76 μm (70%)
Speed	84.6 mm/s (200 in/min)

To embed a fiber, a ball end mill was utilized to cut a slightly oversized pocket to aid in fiber placement and encapsulation. The pocket's depth was slightly less than the fiber's diameter to enhance frictional scrubbing, help promote consolidation, and minimize loads on the fiber. A similar 'no load' fiber embedding method has been presented [16]. Laser machining was not utilized in this study to minimize aluminum oxide formation in the fiber's pocket prior to embedding. To isolate a fiber, additional machining operations were alternated with welding and fiber encapsulation to ensure the embedded fiber was within a representative weld zone of the UAM process. After machining and welding, samples were removed with electrical discharge machining to minimize cutting stresses on the sample and achieve small sample dimensions. Final

[1] 6061-H18 foil as supplied by the vendor was fabricated by cold rolling 6061-O stock material to an H18 temper.

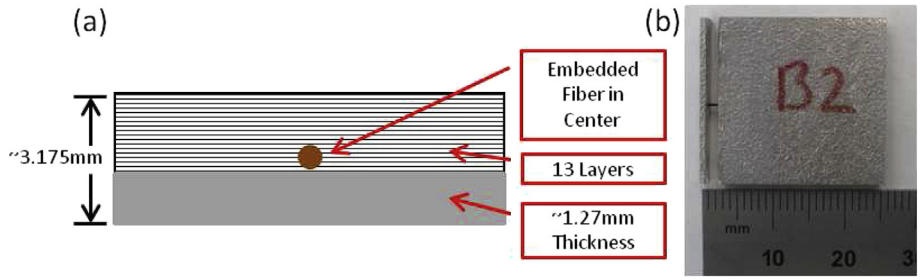

Fig. 3. Sample details: (a) schematic of sample cross section with key fabrication details; (b) physical sample ready to test post manufacture.

samples were near 3.175 mm (0.125″) in thickness and 22.86 mm (0.9″) in width with the NiTi fiber embedded close to center, Fig. 3. The fiber length to pull out from the matrix was chosen to be 1 mm (0.04″) because fiber strain is transferred to the matrix near the edge of the composite due to shear lag [5,17]. Additionally, this length was chosen for feasible manufacturing and handling during testing.

2.2. Fiber pullout testing

Although fiber pullout tests have been detailed in the literature [5,18,19], no standard has been developed for this type of test. A custom fixture was developed and built to fit into square tensile test grips, Fig. 4. This test fixture design was inspired and improved from previous interface strength testing of UAM composites [20,21]. Key features and improvements of this test fixture design are: (i) ability to load samples by sliding them to center, (ii) close fit to a sample's thickness and the use of closely spaced set screws to minimize sample misalignment, rotation, and bending, and (iii) oversized hole drilled at center to minimize fiber misalignment in the testing process. This fixture is made with AISI 1018 Cold Worked Steel to avoid failure and minimize test fixture deformation.

Testing was performed on a TestResources 131R1000-6 load frame with MTS Advantage mechanical wedge type grips and an environmental chamber. The load frame is equipped with a 2.2 kN load cell with a maximum resolution of 1.3 N if all sensor errors are considered. The displacement sensor has a resolution of 0.002 μm. A detailed test setup is shown in Fig. 5. A load rate of 1.27 mm/min (0.05 in/min) was applied to the load frame controller once the sample was secured and aligned within the grips. Due to the somewhat fast load rate, a sampling rate of 250 samples/s was utilized to acquire enough data points. The total travel distance was selected to be 2.54 mm (0.1″) to ensure that the fiber had completely pulled out of the test fixture before the test was stopped. Measured data included time traces of force and distance.

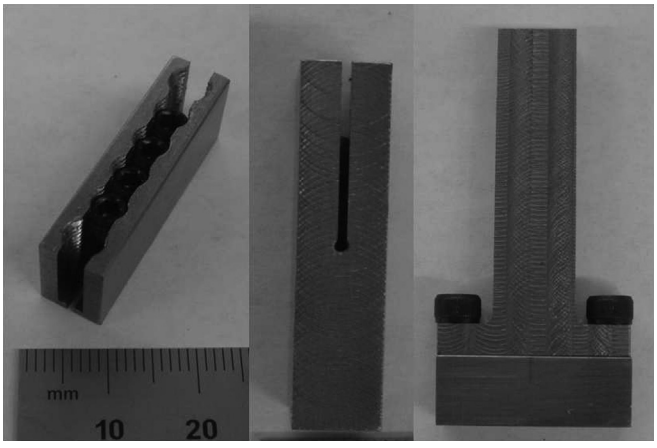

Fig. 4. Custom fiber pullout test fixture used in this study.

2.3. Fiber pullout modeling

In conjunction with fiber pullout testing, a finite element model (FEM) was developed within COMSOL Multiphysics to simulate fiber pullout test conditions. The purpose of this model is to estimate the stress loading in the composite prior to failure, i.e., quantify interfacial stresses, bending loads, and deformation behavior. The model does not incorporate the nonlinear transformation behavior of the NiTi fiber, matrix plasticity, or any residual stresses from the manufacturing process. The model therefore quantifies the interfacial stress behavior up to the point of failure initiation, but not during the failure. It is safe not to incorporate the transformation behavior of the super-elastic wire during pullout testing here because (i) the material utilized experimentally has a high detwinning stress and as such, it will begin to transform when the matrix plastically deforms (see Fig. 6), and (ii) the material cannot physically undergo enough strain to transform into Martensite [13]. Consequently, the NiTi material is modeled in the Austenitic state. Material properties are listed in Table 2[2] while key details and assumptions of the FE construct are shown in Fig. 7. Lastly, to efficiently describe the deformation behavior, a graded mesh made with tetrahedral elements was utilized within the fiber and matrix, Fig. 8. Approximately 10 elements make up the fiber diameter (perpendicular to the fiber's axis) while 40 are used for the axis. The mesh was obtained by refinement until the averaged peak stress (see Section 3) differed less than 2% in magnitude from the previous magnitude over the first 0.12 mm in fiber length.

The FE calculations show that deformation is highly localized around the fiber, as desired, to minimize unwanted bending loads. Displacement around the fiber is large due to the high stress experienced during testing. Localized bending around the fiber does occur, yet the displacements from bending alone are near an order of magnitude smaller than those from fiber loading. Consequently, bending can be assumed not to influence test results.

2.4. Microscopy and microstructure characterization

In addition to mechanical testing and modeling, microscopy analyses were performed to qualitatively and quantitatively study the NiTi–Al interface. Electron and focused ion beam microscopy were performed using a FEI Quanta 200 SEM with EDS capability and FEI Helios NanoLab™ 600 DualBeam FIB/SEM, respectively [22]. Optical images were acquired with an Olympus GX71

[2] Material properties obtained from www.matweb.com and from tensile testing.

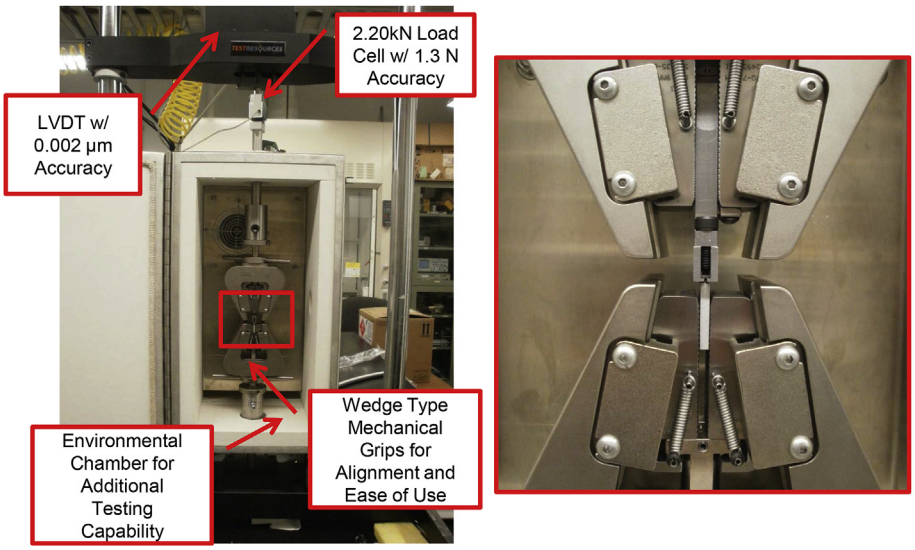

Fig. 5. TestResources load frame used for testing with key specifications listed. The area boxed in red illustrates how the test fixture and sample are loaded into the machine. (For interpretation of the references to color in this figure legend, the reader is referred to the web version of this article.)

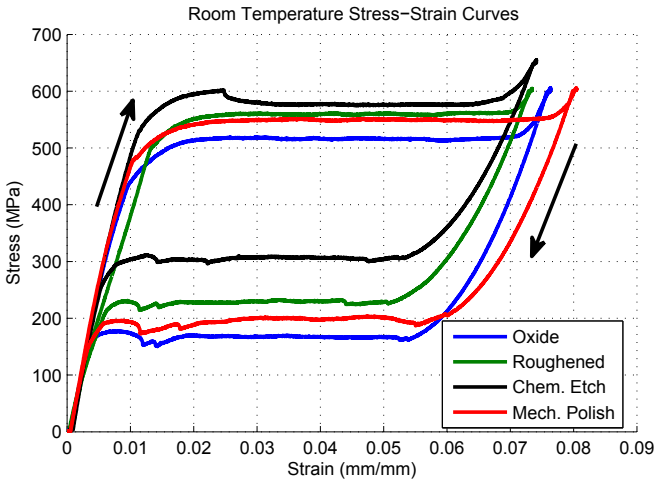

Fig. 6. Room temperature stress–strain curves of nickel titanium fibers utilized in this study. Data was taken using ASTM F2516 - 07e2. The measurements show a high detwinning stress and large elongation to form Martensite.

microscope. SEM imaging was done to evaluate consolidation quality and examine the NiTi–Al interface while simultaneous EDS line scans were performed across various interface regions to quantify diffusion and oxide concentration. Optical and focused ion-beam imaging were performed to analyze grain refinement and failure behavior near a previously embedded mechanically roughened fiber, i.e., the fiber had been pulled out prior to imaging.

SEM Imaging and EDS were done with an electron acceleration voltage of 15–20 keV, a spot size of 4–5 nm, and a working distance of ≈12 mm. EDS scan distance was near 15 μm for all samples while sample spacing was near 1 μm. However, the resolution of the EDS is near 4 μm. Consequently, some data smearing occurs near the interface. Finally, each EDS sample point was measured for 20 s to fully measure energy states of pertinent atoms.

Initially, optical imaging was utilized after etching the aluminum surface with an electrolytic Barker's solution, i.e., near 1% fluoroboric acid, to expose grains [23]. After etching, differential interference contrast (DIC) was utilized to observe the grain

Table 2
FEM material properties.

Property	Al	NiTi
Modulus (GPa)	69	57.5
Poisson's ratio	0.33	0.3
Density (kg/m^3)	2700	6450

structure around the fiber. In order to enhance imaging of small grains formed near the fiber during the UAM process, focused ion beam imaging was utilized to expose grain boundaries by etching away a few nanometers of material at an oblique angle with an accelerating voltage of 30 keV. Ion beam etching works in a similar manner to chemical etchants by exposing grain to grain contrast via grain orientation, yet material removal is more controlled. Once the material is etched away with the ion beam, small grains are more easily imaged with the SEM.

3. Results

3.1. Fiber pullout testing

A representative fiber pullout force-displacement curve and tested oxide surface finish sample are shown in Fig. 9. Key details have been highlighted on the curve to explain test conditions, material behavior, and failure progression. It is emphasized that aluminum remains on the surface of the fiber post failure, which implies matrix rather than interface failure.

Table 3 summarizes fiber pullout test results for the study. All of the samples failed at a similar load level, though differences in the average shear strength can be observed. The average shear stress was calculated by dividing the peak pullout load by the shear area (circumference multiplied by length). Several samples were tested for each surface finish, exhibiting consistent results.

3.2. Fiber pullout modeling

Calculated interfacial shear stresses are shown in Fig. 10. A load of 40 N was applied to the fiber since the experiments show that this load consistently produces failure. Three sample thicknesses

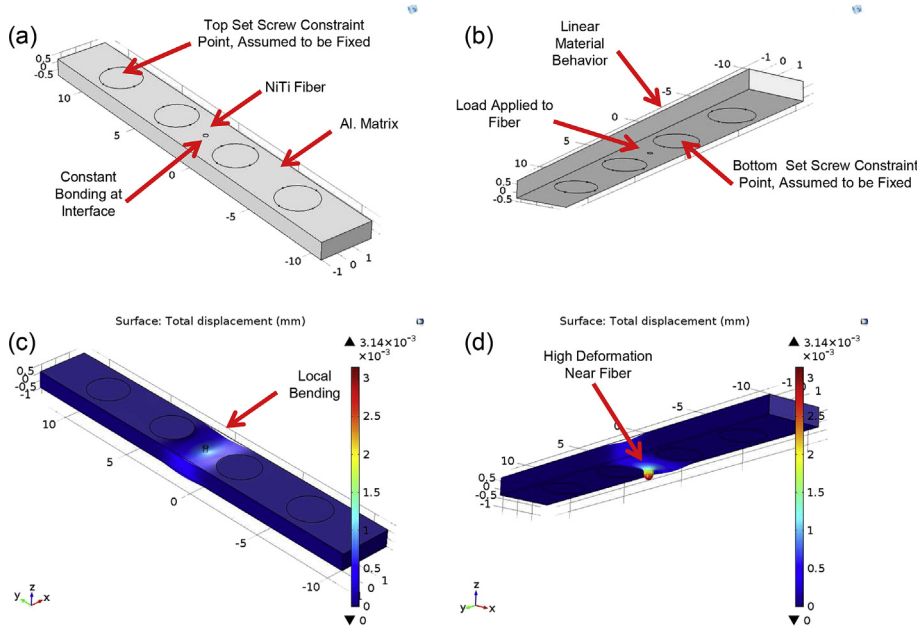

Fig. 7. FE model of fiber pullout test showing key assumptions and details: (a) top view of sample; (b) bottom view of sample; (c) displacement view from top of sample; (d) displacement view from bottom of sample.

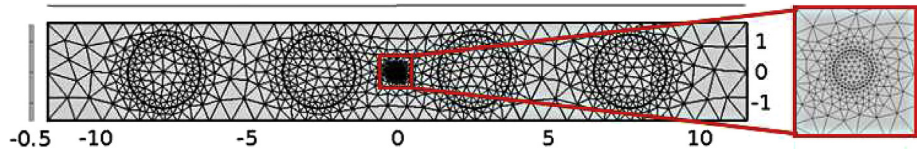

Fig. 8. Graded mesh of FEM with zoomed in region on fiber.

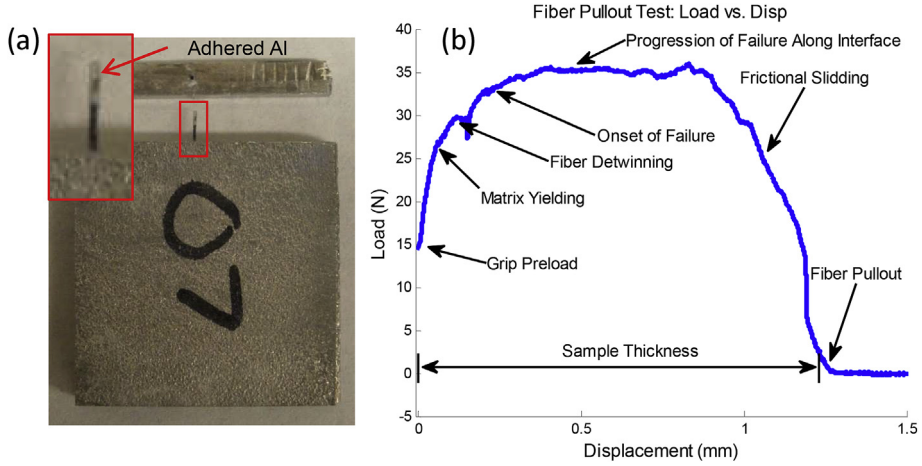

Fig. 9. Representative pullout test result for oxide sample 7: (a) photo of sample after failure illustrating aluminum adhered to surface of fiber; (b) detailed force-displacement pullout test curve.

Table 3
Fiber pullout summary for all surface finishes.

	Oxide	Roughened	Chem. Etched	Mech. Polished
Number of Samples	8	7	3	9
Avg. Peak Pullout Force (N)	37.7	40.5	36.3	37.9
Stdev Peak Pullout Force (N)	5.8	10.7	12.5	9.0
Avg. Sample Length (mm)	1.22	1.02	1.35	1.45
Stdev Sample Length (mm)	0.11	0.20	0.15	0.07
Avg. Shear Stress (MPa)	35.8	45.3	31.1	29.9
Stdev Shear Stress (MPa)	6.7	8.2	12.4	7.5

were considered: 1.0, 1.2, and 1.4 mm. Shear stresses are concentrated near the edge of the sample but they drop off quickly away from the edge due to shear lag between the fiber and matrix. Prior FEM analyses of NiTi composites have shown similar stress profile behavior [24]. As a consequence of the short distance over which the load is transferred from the fiber to the matrix, called the critical fiber length [5], very large localized stresses will be observed, which, in turn, cause failure in a progressive fashion down the fiber. Failure is thus expected to occur at the weakest composite element. Due to the ultimate shear strength of NiTi

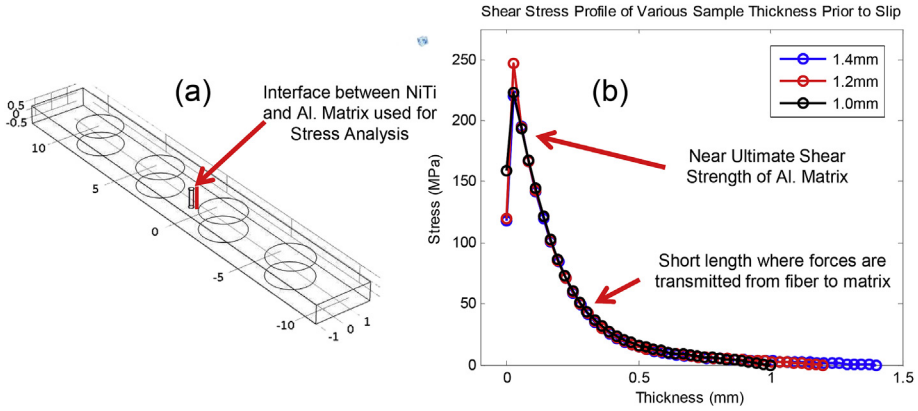

Fig. 10. Shear stress analysis of fiber-matrix interface for 40 N load: (a) stresses were calculated on the line shown; (b) shear stress calculation along the thickness of the aluminum sample, for the three different sample thicknesses considered. Peak stresses are observed to occur at the same depth in the aluminum sample.

(500 MPa) being much larger than the strength of the aluminum tape (150–200 MPa), failure is expected to initiate at the matrix or the interface rather than the fiber.

Table 4 shows the calculated average peak stress and average stress for each sample thickness. The average peak shear stress was calculated by averaging the 5 closest elements to the fiber edge, i.e., the first 0.12 mm of the sample, while the average stress utilized all of the data points. The peak stress was averaged due to the exact peak value being difficult to confidently estimate due to the edge introducing a mathematical singularity in the FEM calculation. Correlation with the experimental data was done by calculating the average shear stress from the ratio of the measured peak pullout force and the total shear area of the fiber. Because of machining variability, each sample had a different thickness: the sample with roughened fiber had a thickness of 1 mm, the oxide sample had a thickness of 1.2 mm, and the mechanically polished sample had a thickness of 1.4 mm. The resulting stresses are shown in the last column of Table 4. The average peak shear stress is largely independent of sample thickness, which, in turn, correlates well with consistently observed failure loads for all samples and smearing of the average shear stress for longer sample thicknesses. Additionally, it is noted that the average peak shear stress is near or above the ultimate shear strength of the aluminum tapes utilized in the UAM process.

3.3. Microscopy and microstructure characterization

3.3.1. Consolidation quality and interface Composition

SEM images of sample cross sections for each surface finish are presented in Fig. 11. These samples were not used in mechanical testing, but were made separately with the same welding conditions as the pullout samples. Tape interfaces cannot be identified easily, which illustrates the consolidation effectiveness of UAM. Additionally, the Al 6061-T6 base plate material can be identified as the area with the slight contrast difference directly below the fiber. Finally, it can be seen that all the fibers were encapsulated well with some void character. Unexpectedly, some of these voids occur near the bottom of the fiber in the oxide and chemically etched surface finishes. This odd bottom of pocket void characteristic could have originated from contaminants on the fiber surface prior to consolidation, which could limit bonding around the fiber. Alternatively, the contaminants could have promoted a corrosive reaction with a chemical utilized in the polishing process.

EDS line scans with corresponding SEM images for the surface finishes of oxide and mechanically roughened are shown in Figs. 12 and 13, respectively. It was found that the mechanically polished and chemically etched surface finishes had similar interface character to the mechanically roughened material, so they are not included for brevity. Fig. 12 shows a uniform oxide layer near 2 micron in thickness that can be observed in the micrograph and in the EDS line scan. On the other hand, no obvious oxide layer can be observed visually or with EDS for the other surface finishes. However, some oxides do appear to become trapped in the surface roughness of the roughened fiber, as seen in Fig. 13. Lastly, for all the surface finishes under investigation, oxygen is observed within the fiber. This oxide is believed to be titanium dioxide which formed post sample polishing.

Table 4
Fiber pullout comparison between FEM and empirical results. Average peak shear stress was computed by averaging first 5 data points near fiber edge while average shear stress averaged all data points over fiber length.

Sample thickness (mm)	Avg. Peak τ (MPa)	Avg. FEM τ (MPa)	Avg. Empirical τ (MPa)
1.0	177.6	46.5	45.3 (Roughened)
1.2	174.2	38.6	35.8 (Oxide)
1.4	168.4	32.6	29.9 (Mech. Polished)

3.3.2. Microstructure characterization

To better understand matrix failure and consolidation character around the fiber, the microstructure was analyzed around a pulled-out mechanically roughened fiber. Optical images of an etched surface using DIC optical microscopy are shown in Fig. 14. The tape interface is observed to crimp around the previously embedded fiber exhibiting large plastic flow. The original tape grain structure consists of long flat grains which result from cold rolling fabrication. These grains appear to flow in and around the fiber due to the circular geometries of the fiber and machined out pocket. Lastly, the tape interfaces can be identified only due to the chemical etchant attacking small grains of similar orientation [25].

The optical images in Fig. 14 give insight into the consolidation microstructure, but the fine grain recrystallization observed at tape [26,27,25] and fiber interfaces [28,29] in the UAM process cannot be clearly distinguished. As a result, FIB imaging was utilized to better characterize and observe this fine grain microstructure. In Fig. 15(a), the microstructure transitions from long flat grains to fine equiaxed grains near the previously consolidated fiber. The flow of aluminum around the fiber and into the pocket can be more clearly seen, as highlighted with arrows, in Fig. 15(b). A crack is observed

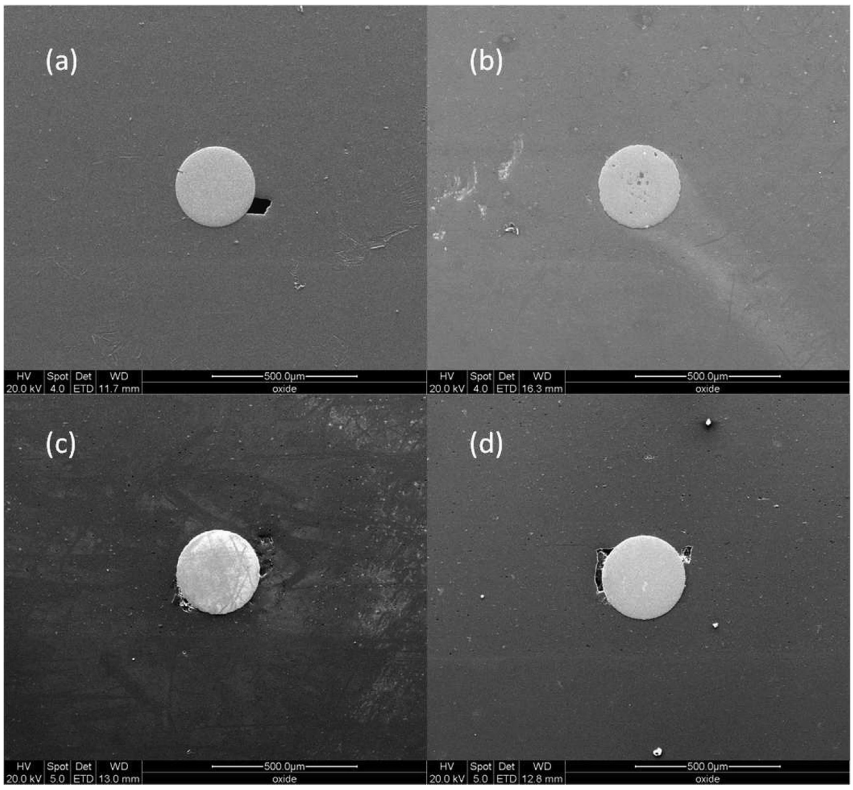

Fig. 11. SEM images of embedded NiTi fibers utilized in this study: (a) oxide surface finish; (b) mechanically roughened surface finish; (c) chemically etched surface finish; (d) mechanically polished surface finish.

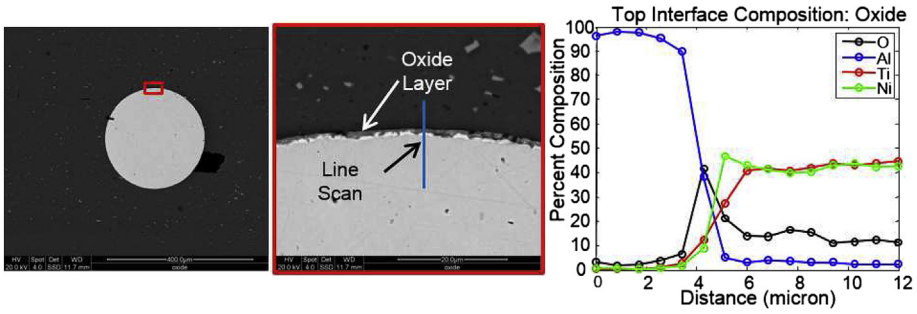

Fig. 12. SEM image of top of oxide surface finish fiber with corresponding EDS line scan.

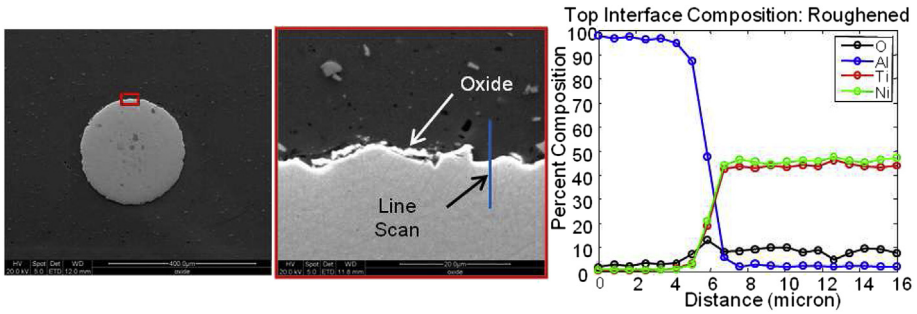

Fig. 13. SEM image of top of mechanically roughened surface finish fiber with corresponding EDS line scan.

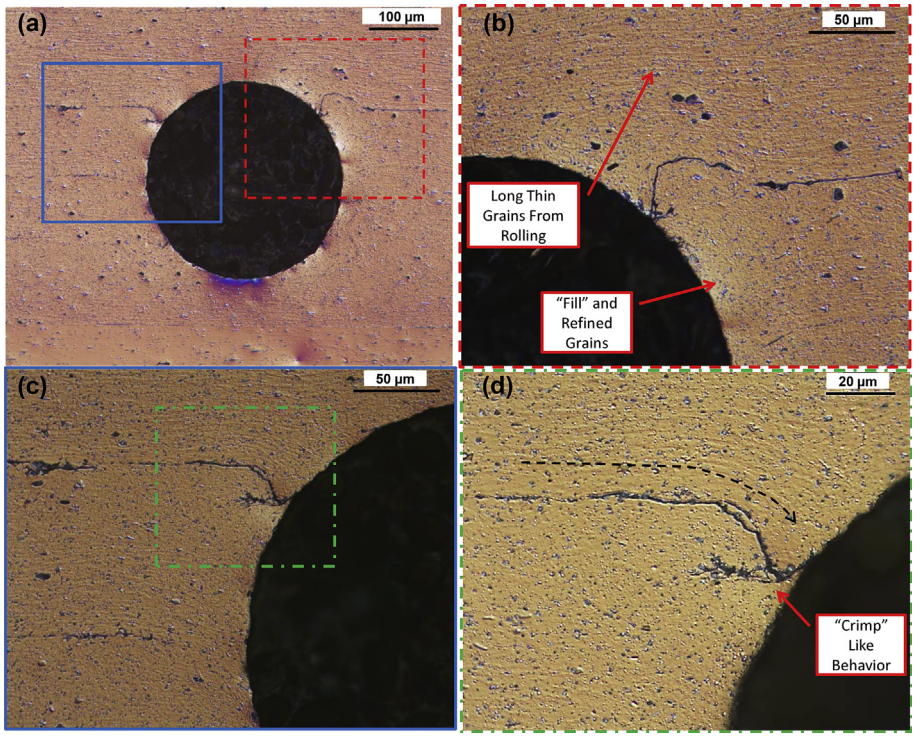

Fig. 14. Optical images of etched sample at various magnifications using DIC to show grain structure around pulled out fiber: (a) overall view; (b) right top and side; (c) left top and side; (d) zoomed-in left side.

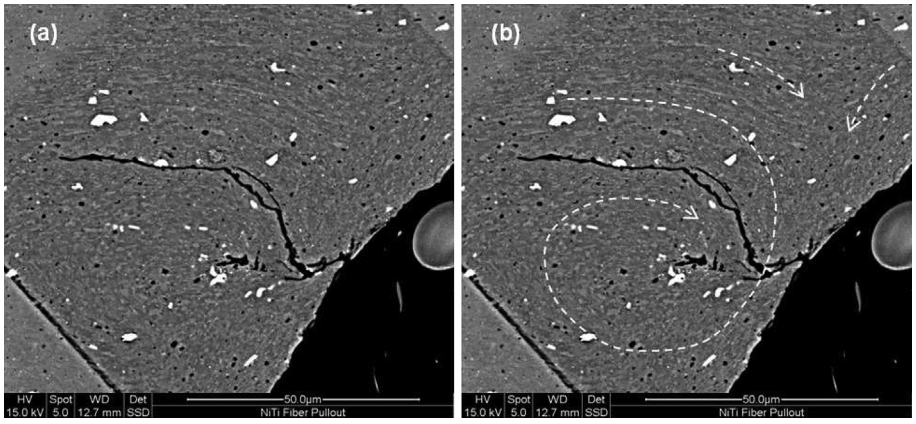

Fig. 15. Focused ion beam etched surface: (a) grain structure without flow detail; (b) grain structure with flow detail.

along the tape crimp, which likely formed during mechanical testing and was intensified once a chemical etchant was utilized. No obvious cracks were observed in the pristine NiTi–Al composite, see Fig. 16.

4. Discussion

In order to understand and improve the fiber–matrix interface in UAM metal-matrix fiber composites, fiber pullout tests were developed to estimate interfacial shear stress and study failure behavior near room temperature. It was found that fiber surface condition did not play a significant role in strengthening the interface because plastic deformation occurred in the matrix prior to the NiTi–Al interface breaking for each surface finish type. Failure of the matrix was evidenced by adhered aluminum seen on all samples after pullout. Further, failure occurred at very similar load levels for each surface finish. In conjunction with fiber pullout testing, a finite element model was developed within COMSOL to analyze sample loading prior to failure. The FEM calculations support plastic deformation of the matrix due to stress levels being above its ultimate shear strength. High shear stress occurs within the matrix because of shear lag effects, i.e., the narrow region of strain transfer from the fiber to the matrix creates a stress concentrator. As a result of high shear loading for all surface finishes, the matrix fails before the NiTi–Al interface.

Microscopy analysis shows that all fiber surface finishes can lead to consolidation with little void presence. For the oxide surface finish, it is observed that little to no metallic bonding takes place due to the consistent, unbroken, oxide layer on the fiber. Instead, nearly all interactions between the matrix and fiber would come

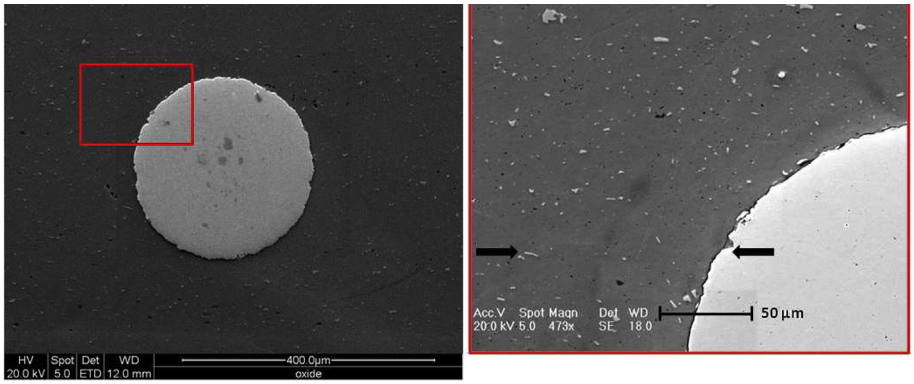

Fig. 16. Analysis of pristine roughened NiTi fiber prior to pullout. Arrows identify the approximate tape interface.

from friction or mechanical interlocking. On the other hand, the other surface finishes show no observable oxide layer, which could imply metallic bonding. However, no measurable diffusion is observed at the interface due to the fast weld time and low formation temperature of the UAM process. Consequently, it cannot be confidently said what the exact bond constituents are for the mechanically roughened, chemically etched, or mechanically polished surface finishes.

The microstructure of a failed sample was analyzed using optical, FIB, and SEM imaging to understand why the aluminum matrix failed and not the NiTi–Al interface. It was determined that large plastic flow of the aluminum matrix around the recessed embedded fiber forced the tape interface to crimp and create a large zone of recrystallized grains. Due to these characteristics, a robust bond is formed around the fiber which entails micron and submicron sized grains. Additionally, because micron and submicron grains are formed around the fiber during construction, it is likely that grains near in size compared to fiber surface asperities were able to form. As a result, the matrix would fail via shear because submicron grains would become trapped within the asperities of the fiber, which, in turn would lead to robust mechanical interlocking and high resistance to shear at the NiTi–Al interface. Similar to the EDS line scans, it cannot be confidently said that all of the surface finishes failed via subgrain entrapment, but this idea is consistent with the oxide surface finish due to the limited possibility of metallic bonding.

5. Concluding remarks

In summary, interfacial shear stress and bond mechanisms were studied as a function of NiTi fiber surface finish for NiTi–Al UAM composites with the use of fiber pullout testing and microscopy. This study was carried out to improve and understand the NiTi–Al interface for improved design and modeling of NiTi–Al composites due to previous work showing proof of interface failure and frictional bonding between the matrix and fiber. With this study, strong evidence is presented that the matrix is in fact the weakest link in the composite for all surface finishes due to consistent observation of remaining aluminum on pulled out fibers and simulated peak shear stress being near or above the welded aluminum tape's shear strength. Consequently, bond mechanisms for all fiber surface finishes supersede the strength of the aluminum matrix and show that there is no clear optimal surface finish. However, with the use of stronger matrices or characterization of the interface at elevated temperatures, surface finish may play a larger role in failure.

It has also been confirmed from previous work that the UAM process does not break up the oxide layer on the oxide surface finish fiber and that the bond mechanism is largely a mechanical interlock or a friction fit. The other surface finishes have no observable oxide layer that would prohibit metallic bonding. Thus, it is possible that metallic bonding may be taking place. Although the exact bond mechanisms cannot be determined for each fiber, the mechanically roughened fiber appears to be the best from a potential bond strength perspective because it offers both increased frictional coupling and the possibility of metallic bonding.

Lastly, microstructure examination around a failed mechanically roughened fiber was carried out to investigate why matrix failure occurred. It was found that large plastic flow of the matrix during the UAM process crimps the tape interface and provides a kinetic path for dynamic recrystallization of the aluminum, i.e., favorable grain refinement of the aluminum around the fiber. Due to the matrix near the fiber recrystallizing, micron and submicron equiaxed grains are formed, which are similar in size to the surface asperities of the consolidated fibers. As a result, small grains could become entrapped within these asperities which significantly enhance the mechanical interlocking and pullout resistance for all surface finishes.

Acknowledgments

Support for A.H. comes from a National Science Foundation Graduate Fellowship under Grant No. 1102690. Any opinions, findings, and conclusions or recommendations expressed in this material are those of the authors and do not necessarily reflect the views of the National Science Foundation. The authors acknowledge the financial support from the member organizations of the Smart Vehicle Concepts Center (www.SmartVehicleCenter.org), a National Science Foundation Industry/University Cooperative Research Center. The technical assistance of Phillip Evans (MIT Lincoln Laboratory), Walter Green (OSU), Ross Baldwin (OSU), Cameron Begg (OSU), and Dan Huber (OSU) is acknowledged.

References

[1] Graff K. Ultrasonic additive manufacturing. American Society for Metals International; 2011.
[2] Graff K, Short M, Norfolk M. Very high power ultrasonic additive manufacturing (VHP UAM). In: International solid freeform fabrication symposium; 2011. Austin, TX.
[3] Hahnlen R. Characterization and modeling of Active metal-matrix composites with embedded shape memory alloys [Ph.D. thesis]. Columbus, OH: The Ohio State University; 2012.
[4] Hahnlen R, Dapino M. NiTi-al interface strength in ultrasonic additive manufacturing composites. Compos Part B Eng 2014;59:101–8.

[5] Chawla K. Composite materials: science and engineering. Springer; 1998.
[6] Jonnalagadda K, Kline G, Sottos N. Local displacements and load transfer in shape memory alloy composites. Exp Mech 1997;37(1):78–86.
[7] Smith N, Antoun G, Ellis A, Crone W. Improved adhesion between nickel-titanium shape memory alloy and polymer matrix silane coupling agents. Compos Part A 2004;35:1307–12.
[8] Poon C, Lau K, Zhou L. Design of pull-out stresses for prestrained SMA wire/polymer hybrid composites. Compos Part B 2005;36:25–31.
[9] Wang X, Hu G. Stress transfer for a SMA fiber pulled out from an elastic matrix and related bridging effect. Compos Part A 2005;36:1142–51.
[10] Rossi S, Deflorian F, Pegoretti A, D'Orazio D, Gialanella S. Chemical and mechanical treatments to improve the surface properties of shape memory NiTi wires. Surf Coatings Technol 2008;202:2214–22.
[11] Hamming L, Fan X, Messersmith LBPB. Mimicking mussel adhesion to improve interfacial properties in composites. Compos Sci Technol 2008;68:2042–8.
[12] Sadrnezhaad S, Nemati N, Bagheri R. Improved adhesion of NiTi wire to silicone matrix for smart composite medical applications. Mater Des 2009;30:3667–72.
[13] Payandeh Y, Meraghni F, Patoor E, Eberhardt A. Effect of martensitic transformation on the debonding propagation in Ni-Ti shape memory wire composite. Material Sci Eng A 2009;518:35–40.
[14] Center for ultrasonic additive manufacturing (June 2014). URL https://uam.engineering.osu.edu/.
[15] Wolcott P, Hehr A, Dapino M. Design of experiment for optimal build parameters for high power ultrasonic additive manufacturing of Al 6061. In: SPIE smart structures/NDE, San Diego,CA; 2014.
[16] Kong C, Soar R. Fabrication of metal–matrix composites and adaptive composites using ultrasonic consolidation process. Mater Sci Eng A 2005;412(1–2):12–8.
[17] Li. Z.-F, Grubb. D. T, Single-fibre polymer composites: Part I Interfacial shear strength and stress distribution in the pull-out test, J Material Sci 29.
[18] Marshall. D, Shaw. M, Morris. W, Measurement of interfacial debonding and sliding resistance in fiber reinforced intermetallics, Acta Metallurgica Materialia 40(3).
[19] Kerans. R, Parthasarathy. T, Theoretical analysis of the fiber pullout and Pushout test, J Am Ceram Soc 74(7).
[20] Kong C, Soar R, Dickens P. Ultrasonic consolidation for embedding sma fibres within aluminium matrices. Compos Struct 2004;66:421–7.
[21] Li. D, Soar. R. C, Characterization of process for embedding SiC fibers in Al 6061 O matrix through ultrasonic consolidation, J Eng Mater Technol 131.
[22] Center for electron microscopy and analysis (cemas) (June 2014). URL http://cemas.osu.edu/.
[23] ASM handbook: volume 9 metallography and microstructures. American Society for Materials International; 1985.
[24] Wang Y, Zhou L, Wang Z, Huang H, Ye L. Analysis of internal stresses induced by strain recovery in a single SMA fibermatrix composite. Compos Part B 2011;42:1135–43.
[25] Fujii H, Sriraman M, Babu S. Quantitative evaluation of bulk and interface microstructures in Al-3003 alloy builds made by very high power ultrasonic additive manufacturing. Metallurgical Mater Trans A Phys Metall Mater Sci 2011;42(13):4045–55.
[26] Johnson K. Interlaminar subgrain refinement in ultrasonic consolidation [Ph.D. thesis]. Loughborough, UK: Loughborough University; 2008.
[27] Dehoff R, Babu S. Characterization of interfacial microstructures in 3003 aluminum alloy blocks fabricated by ultrasonic additive manufacturing. Acta Mater 2010:1–12.
[28] Li D, Soar RC. Plastic flow and work hardening of Al alloy matrices during ultrasonic consolidation fibre embedding process. Mater Sci Eng A 2008;498(1–2):421–9.
[29] Friel RJ, Harris RA. A nanometre-scale fibre-to-matrix interface characterization of an ultrasonically consolidated metal matrix composite. Proc Institution Mech Eng Part L J Mater Des Appl 2010;224(1):31–40.